Magn Reson Mater Phy (2009) 22:257–265
DOI 10.1007/s10334-009-0172-4

RESEARCH ARTICLE

Monitoring the survival of islet transplants by MRI using a novel technique for their automated detection and quantification

Daniel Jirak · Jan Kriz · Michal Strzelecki · Jiabi Yang · Craig Hasilo · David J. White · Paula J. Foster

Received: 4 November 2008 / Revised: 3 April 2009 / Accepted: 6 April 2009 / Published online: 24 April 2009

Abstract
Object There is a clinical need to be able to assess graft loss of transplanted pancreatic islets (PI) non-invasively with clear-cut quantification of islet survival. We tracked transplanted PI in diabetic mice during the early post-transplant period by magnetic resonance imaging (MRI) and quantified the islet loss using automatic segmentation technique.
Materials and methods Magnetically labeled islet iso-, allo- and xenografts were injected into the right liver lobes. Animals underwent MRI scanning during 14 days after PI transplantation. MR images were processed using custom-made software, which automatically detects hypointense regions representing PI. It is based on morphological top-hat and bottom-hat transforms.
Results Manually and automatically detected areas, corresponding to PI, differed by 4% in phantoms. Signal loss regions due to PI decreased comparably in all groups during the first week post transplant. Throughout the second week post-transplant, the signal loss area continued in a steep decline in case of allografts and xenografts, whereas the decline in case of isografts slowed down.
Conclusion Automatic segmentation allows for the more reproducible, objective assessment of transplanted PI. Quantification confirms the assumption that a significant number of islets are destroyed in the first week following transplantation irrespective of allografts, xenografts or isografts.

Keywords Magnetic resonance imaging (MRI) · Pancreatic islets (PI) · Quantification · Automatic segmentation · Animal model

D. Jirak · J. Kriz · P. J. Foster (✉)
Imaging Research Laboratories, Robarts Research Institute, London, ON N6A 5K8, Canada
e-mail: pfoster@imaging.robarts.ca

D. Jirak
e-mail: daji@medicon.cz

J. Kriz · J. Yang · C. Hasilo · D. J. White
Transplantation Group, Robarts Research Institute, London, ON, Canada

M. Strzelecki
Institute of Electronics, Technical University of Lodz, Lodz, Poland

P. J. Foster
Department of Medical Biophysics, University of Western Ontario, London, ON, Canada

Introduction

Pancreatic islet (PI) allotransplantation has been exploited as an alternative treatment of Type-1 diabetes in hypoglycemia unaware diabetic patients [1,2]. Some estimate that 60%, or more, of PI transplanted by portal vein infusion are destroyed within the first two days [3–7]. In addition, the initial high number of patients (∼80 %) independent of exogenous insulin decreases to ∼15% 5 years after transplantation [8]. Thus there is a strong clinical need to be able to assess graft loss non-invasively with clear-cut quantification of PI survival.

The experimental visualization of iron labeled cells in vivo with cellular MRI has become routine [9–13] with detection now at the single cell level [14,15]. Iron labeled cells appear as regions of signal loss in MR images. A number of studies have now provided evidence that cellular MRI can be used to detect and monitor transplanted islets in vivo in animal models [16–20]. However, it is not always possible to identify and quantify the iron labeled cells unambiguously. The goal of this work was to further develop our cellular MRI technology to permit measurements of PI graft survival and rejection. Here we present a simple and robust method, which

allows the in vivo quantification of labeled PI in MR images. Our results on phantoms suggest that the technique described here will allow for the reproducible, more objective assessment of transplanted PI. We have applied our approach to the task of tracking transplanted allo-, xeno- and isografts of PI in diabetic mice during the early post-transplant period.

Materials and methods

All protocols used in this study were approved by the University of Western Ontario Animal Care Committee and were conducted in accordance with the policies contained in the Canadian Council on Animal Care.

Pancreatic islet isolation, labeling

Pancreatic islets were isolated from adult male C57BL/6 and BALB/c mice and Lewis rats (Charles River Laboratories, Inc., Canada) using a modified technique described by Gotoh et al. [20]. Briefly, islets were obtained after distension of the pancreas by collagenase solution (Collagenase V, Sigma-Aldrich, USA, 1 mg/ml mice 3 ml for mice, 15 ml for rats) followed by 10–15 min incubation at 37°C and purification using a discontinuous density gradient (islet gradient 1.037, 1.069, 1.096, 1.108 g/ml; Mediatech, Inc., USA). Isolated PI were labeled with superparamagnetic iron oxide (SPIO) nanoparticles by incubation overnight in CMRL-1066 medium (37°C, 5% atm. CO2; HyClone, USA) with 10% fetal calf serum, 1% HEPES, 1% L-glutamine, 1% antibiotics (penicillin 10,000 IU/ml; streptomycin 10 mg/ml, all from Sigma-Aldrich, USA) and the SPIO MRI contrast agent Feridex® (Berlex Laboratories, Canada) complexed with poly-L-lysine (PLL, Sigma-Aldrich, USA) (25.0 µg Fe/ml: 15 µl/ml PLL). We followed the protocol used previously in our lab, which resulted in normal insulin secretion and excellent viability [11]. Feridex labeled islets were transferred from a tissue culture flask to a 50 ml tube with fresh tissue culture media and allowed to gravity sediment for 10 minutes. Settled down islets were then transferred to a dark glass dish and handpicked under a surgical microscope using a 27G shielded winged needle connected to 1 ml syringe (Becton Dickinson, Mexico).

Gel samples were prepared for imaging by placing 1–10 labeled and unlabeled PI in a 350 µl well, in a single plane sandwiched between two layers of gelatin; the bottom layer was 4% (w/w) gelatin and the top layer was 2% gelatin. Other gel samples consisted of 100–400 labeled PI in a 50 ml tube in a single plane sandwiched between two layers of gelatin; the bottom layer was 4% (w/w) gelatin and the top layer was 3% gelatin. Images from these phantoms were used to validate the quantification methodology.

Experimental animals, pancreatic islet transplantation

Diabetes was induced by the intraperitoneal administration of streptozotocin (220 mg/kg, Sigma-Aldrich, USA), 7 days before transplantation. Blood glucose levels were measured daily during the first week post-transplant and every other day during the second week post-transplant. Blood glucose levels over 18 mmol/l, on two consecutive days, were considered to indicate diabetes.

Two-month-old BALB/c male mice (inbred strain, 20–22 g, Charles River Laboratories, Inc., Canada) were used as PI recipients. Three transplant groups were studied: allografts ($n = 4$ C57BL/6 mouse donors), xenografts ($n = 3$ Lewis rat donors) and isografts ($n = 6$ BALB/c mouse donors). Healthy BALB/c mice were used as controls: five untouched mice, two mice received unlabeled PI and three mice received free iron (concentration equivalent to approximately 230 labeled islets according to Tai et al. [11]) via the same delivery methods described below.

Two hundred to three hundred Feridex labeled and purified PI were injected into the right liver lobes of diabetic mice using an approach described by Yonekawa et al. [21]. In this novel transplantation model the left hepatic branch of the portal vein is temporarily clamped and PI are injected into the ileocaecal vein. Briefly, mice were anesthetized for transplantation using inhalational anesthesia (3% isoflurane in oxygen for induction, 1.5% for maintenance). Buprenorphine (0.03 mg/kg) was injected subcutaneously at the beginning of surgery. The mouse recipient abdomen was opened by a midline laparotomy, the left hepatic branch of the portal vein was temporarily clamped with a Micro Serrefine clip (Fine Science Tools GmbH, Germany) and the PI were subsequently injected into the ileocaecal vein in 500 µl of media. The tip of the needle was covered by microfibrillar collagen hemostat (Avitene, Bard Canada) before being removed, and gentle pressure was applied to the puncture to stop the bleeding. Twenty seconds after the PI injection, the vascular clamp was removed and the full liver blood supply re-established. The color of the liver tissue normalized rapidly. The abdominal wall was closed in two layers using continuous suture (5-0 silk, Johnson & Johnson, USA).

MR imaging

Imaging was performed on a 3T MRI scanner (GE Medical Systems, USA) using a custom-built, high-performance gradient coil insert and a customized whole mouse body solenoid radiofrequency coil (3 cm diameter, 5 cm length). Images were acquired using a 3D fully refocused (steady-state free precession) gradient-echo sequence (known as FIESTA on GE scanners) with the following parameters: repetition time (TR) = 3.8 ms, echo time (TE) = 1.8 ms, flip angle (FA) = 25°, bandwidth = 62.5 kHz, field of view (FOV) = 4×4 cm^2.

The scanned resolution was $200 \times 200 \times 200\ \mu m^3$. Zero filling was used to give an interpolated voxel dimension of $78 \times 78 \times 100\ \mu m^3$. The scan time was 25 min for mice (3 min for gel phantoms). Mice were anesthetized during imaging using isofluorane (3% for induction, 1% for maintenance). Automatic segmentation techniques was also tested on phantoms containing 100–400 PI scanned on a 4.7 T Bruker spectrometer (Bruker BioSpec, Germany) using resonator coil (7 cm diameter, Bruker BioSpin, Germany). Images were acquired using turbo spin echo (RARE) sequence (TR = 3000 ms, TE = 36 ms, FOV = $4.5 \times 4.5\ cm^2$, turbo factor = 8) and fast low-angle gradient echo (FLASH) sequence (TR = 100 ms, TE = 3.7 ms, FOV = $4.5 \times 4.5\ cm^2$). Plane resolution was $176 \times 176\ \mu m^2$ for both types of sequence. To change a fractional signal loss of labeled PI, and image signal-to-noise ratio, the slice thickness varied between 0.85 and 4 mm, and number of acquisitions varied between 1 and 16.

Image processing, detection and quantification of pancreatic islets

Image signal to noise ratio was measured as the mean signal intensity (SI) in the kidney cortex divided by the standard deviation of the signal from noise in background air. MR images were converted to bitmap format (BMP, 256 grayscale) and processed using an in-house program, written in Matlab (The Mathworks Inc, USA), which detects hypointense regions representing PI independently of the user. The first step was the automatic enhancement of contrast between the regions of signal loss and the liver tissue. This was based on morphological top-hat and bottom-hat transforms [22,23]. Briefly, the top-hat transform is defined as the residuum between the original image and its opening. The opening of an image results in removing small bright details, which are smaller than size of the structuring element. Other image regions will remain unchanged. The shape and size of this structuring element define which bright objects will be removed from the original image. Thus, the top-hat transform (as a difference between original and opened image) emphasizes these bright objects, providing at the same time equalization of image background. Similarly, the bottom-hat transform is defined as the difference between the image closing and the original one. The closing of an image, opposite to its opening, ensures erasing small dark objects, smaller than the size of structuring element. In consequence, the bottom-hat transform results in small dark image details on reasonably even background. Combining these operations together, i.e. adding the original image to its top-hat transform and subtracting the bottom-hat transform from the result leads to image enhancement. The shape of the structuring element was set experimentally, based on the size and shape of the analyzed islets in MR images of phantoms and livers, as the circle and its diameter was 4 pixels which corresponds to the smallest observed hypointense area due to labeled PI in gel samples. The shape and size of that element was the same for all analyses.

In the second step, a histogram of the entire image slice was generated and a threshold was automatically determined for the identification of regions of signal loss due to transplanted PI in each slice. The threshold was based on image histogram and was set as the first local minimum signal intensity value, representing the point between the signal intensities of the background and foreground tissues. The pixels within the liver tissue with signal intensity values below this threshold were considered to be PI. If the threshold differed by more than 15% in two neighboring slices, a weighted average was calculated from the currently analyzed image slice (weight = 0.30) and the five previous slices (weight = 0.14) to minimize the segmentation error. As a result of the thresholding, all pixels identified as regions of signal loss were re-assigned to a zero signal intensity (black pixels). Images of labeled PI in gelatin samples, and in vivo in mouse liver, before and after application of this processing, are shown in Fig. 1. The liver was outlined manually by experienced investigators to eliminate false positive findings originating from the tissue outside the liver and the black pixels (signal intensity = 0) within the liver tissue were counted automatically using ImageJ software (NIH, USA).

Histology

Animals were killed 2 weeks after transplantation and their livers excised for histological examination. Liver tissue was fixed in 10% buffered formalin for 2 days, embedded in paraffin, and 5-μm thick sections were subsequently stained with hematoxylin and eosin (H&E) standard techniques. For insulin immunohistochemistry tissue sections were heated in the microwave with citric acid buffer (10 μm, pH 6.0) to unmask the antigen. All sections were blocked by 10% normal horse serum (Vector Laboratories, Burlingham, CA) and a peroxidase blocking reagent (Dako, Carpinteria, CA). The guinea pig anti-human insulin (Abcam, Cambridge MA, USA) was diluted to 1:50, then incubated for 60 min at room temperature (RT). After washing, the sections were incubated with rabbit EnVision+ polymer-HRP (Dako, Carpinteria, CA) for 30 min at RT. The sections were rinsed in PBS and were stained in DAB solution (Dako, Carpinteria, CA) for 2–5 min at RT, and counterstained with hematoxylin.

Statistical analysis

Differences in the area of signal loss in the liver tissue in the three transplant groups were determined using the Student *t* test assuming equal variances. The three transplant groups were compared using one-way ANOVA with Tukey's

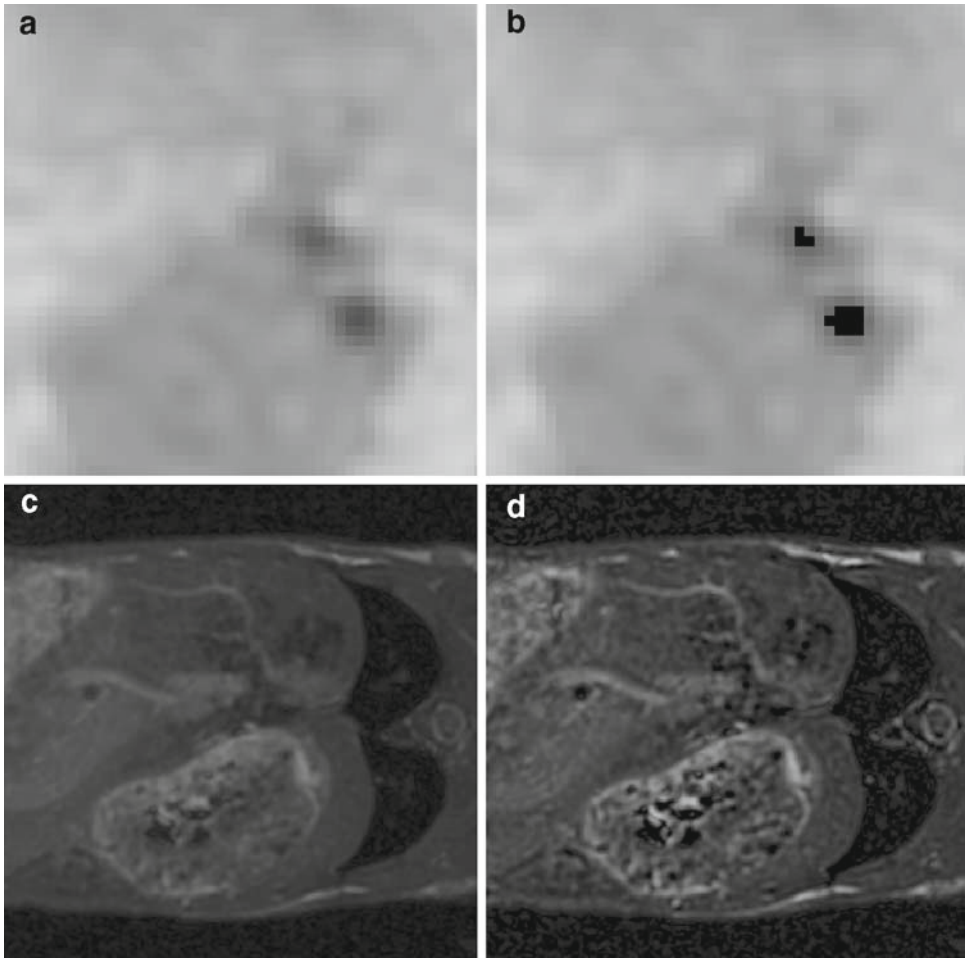

Fig. 1 MR images of labeled islets in the phantom and in the mouse liver. Images of labeled islets in gelatin are shown before (**a**) and after (**b**) the segmentation and thresholding process. Images of labeled islets in the mouse liver are shown before (**c**) and after (**d**) the automatic contrast enhancement used for thresholding

post hoc test (statistical program GraphPad Prism, USA). A value of $P < 0.05$ was considered statistically significant.

Results

Imaging of PI in gel samples, validation of automatic segmentation methods

To validate the automated segmentation method, MR imaging was first performed on gel samples containing 1 to 10 labeled PI (Fig. 1). The PI were visible as hypointense regions (Fig. 1a), the mean fractional signal loss was $54 \pm 3\%$. The total area of signal loss detected in the images of labeled PI in gelatin by the automatic segmentation method (Fig. 1b) was $96 \pm 9\%$ of that outlined manually by three different trained personnel. No area of signal loss was detected in gel samples containing non-labeled PI. More detailed analysis for validation of automatic segmentation technique was performed on gel samples containing 100–400 PI. Islets were automatically detected if fractional signal loss of area corresponding to PI was 30% or higher. In case of images acquired with high image signal-to-noise ratio (30–130), the standard deviation of automatic detected area of signal loss was 4.7%. For lower signal-to-noise ratio, the automated segmentation method failed: for example for signal-to-noise ratio between 4 and 14, the standard deviation of automatic detected area of signal loss was 51.1%. We also determined the inter observer variability by comparing the evaluation of the same images without and with automatic segmented area. Five persons assigned the PI area in three different images, each six times. Without automatic segmentation, the standard deviation of detected area corresponding to PI was 30.6% ($n = 5$) and the inter-observer variability was in the range of 4.5–29.4% (the mean standard deviation in person was 13.6%). After automatic segmentation, all experts obtained the same results regarding the PI area, thus the inter observer variability was 0%.

In vivo imaging of PI

Mice were imaged at 3T on days 1, 3, 5, 7, 10 and 14 post-transplantation. The image quality was high with a mean signal-to-noise ratio of at least 40 (measured in the kidney

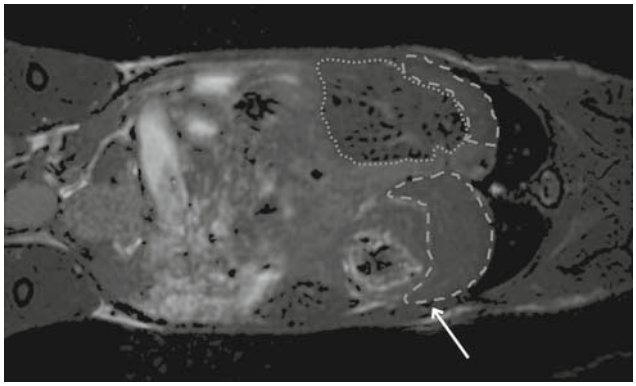

Fig. 2 Automatic detection of transplanted islets in the mouse liver. In vivo MRI of the mouse liver one day after allogeneic transplantation into the right lobe (*dotted line*). Segmented pancreatic islets in the transplanted lobes appear as *black* voids. No islets were detected in the control liver tissue (*dashed line*). The liver was outlined manually to eliminate false positive findings, for example the hypointense signal from the bone of rib (*arrow*)

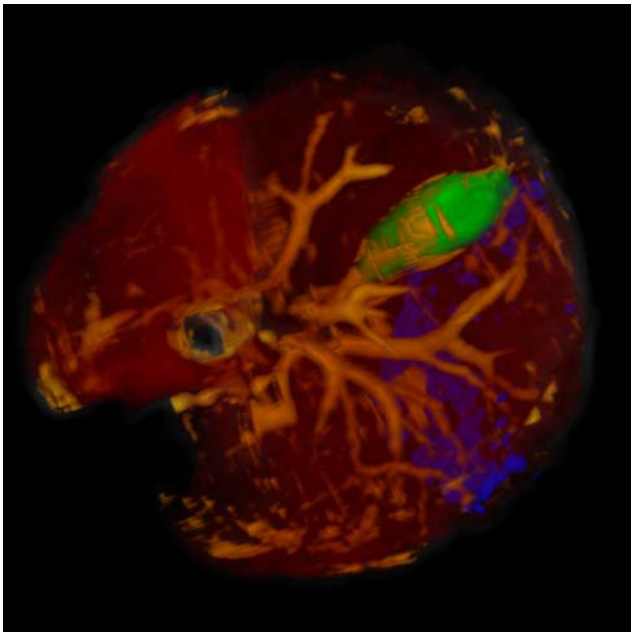

Fig. 3 3D distribution of transplanted PI (*blue*) in the liver (*red*) obtained with in vivo MRI. *Green* gall bladder, *yellow* veins

cortex). In all transplanted mice the regions of signal loss, attributed to PI, were detected in the right liver lobes on coronal MR images of the mouse body, confirming the technical success of transplantation (Fig. 2). Regions of signal loss attributed to PI were not observed in the non-transplanted control left lobes of the PI recipients or in the liver of mice that received unlabeled PI or free iron (data not shown). By transplanting PI into a specific and known portion of the liver only, the regions of signal loss caused by PI could be readily identified while the liver lobes which were free of PI served as control tissue in the same animal. This is best visualized in a 3D representation of the image data where the transplanted PI are depicted as blue spots (Fig. 3).

On day 1, the average volume of the voxels representing PI was 34.4 ± 19.3 µl. This represents approximately 3% of the whole liver volume [24]. This is larger than the actual volume of the transplanted tissue and is due to what is known as the blooming artifact, an effect which causes the signal loss generated in MR images to be much larger than the actual area occupied by the iron-labeled cells [25].

Quantification of the transplanted islets

The total volume of signal loss measured in the transplanted lobes of the liver on the first day after transplantation was rated as 100% and subsequent measurements were recalculated as relative numbers. Mean values for the cumulative decline of signal loss at each imaging time point are given in Table 1. There was a dramatic decrease in the total volume of signal loss in all three groups. A statistically significant decrease in the total volume of signal loss was observed 3 days after transplantation, in animals of both the allograft and isograft groups, and 5 days after transplantation in the xenograft group ($P < 0.05$). The mean cumulative decline of signal loss was comparable in all groups after the first week post-transplant. The total volume of signal loss continued to decline in transplanted livers of all mice over the 2-week observation period. However, in the second week post-transplant, regions of signal loss due to allografts and xenografts continued to rapidly decline. A significant difference was found between days 7 and 14, for the allografts ($26.3 \pm 7.4\%$) and xenograft ($19.2 \pm 4.0\%$) group ($^{\ddagger}P < 0.05$). Regions of signal loss due to allografts declined $4.4 \pm 1.3\%$ per day, due to xenografts $2.75 \pm 0.4\%$ per day, and due to isografts $1.1 \pm 0.2\%$ per day.

Functioning of labeled pancreatic islets

Non-fasting blood glucose levels normalized by day 1 post-transplant. This confirms that labeled PI continue to function which corresponds to previously reported results [11]. While isografts maintained normoglycemia until the end of the study (day 14), the function of allografts and xenografts failed 10 ± 3 days after transplantation. Mice in the isograft group underwent partial hepatectomy on day 17 to remove the right liver lobes with transplanted PI. All of these mice became hyperglycemic within the next 3 days demonstrating that it was the transplanted PI that were maintaining glucose homeostasis (data not shown).

Table 1 Decline in regional signal loss (%)

Animal group	Days after transplantation					
	1	3	5	7	10	14
Allograft	100	85.1 ± 8.8*	71.8 ± 7.0	62.4 ± 8.8	45.5 ± 9.2	36.2 ± 4.3†‡
Isograft	100	80.6 ± 13.3*	62.7 ± 13.7	50.1 ± 9.8	47.4 ± 9.2	41.9 ± 9.7
xenograft	100	77.2 ± 23.9	66.8 ± 16.2*	54.3 ± 5.1	46.9 ± 9.7	35.1 ± 8.9†‡

Decline in regional signal loss (mean ± SD), relative to day 1, in the three different transplant groups. A significant decrease, compared to the initial values, occurred at 3 days after transplantation in allograft and isograft groups and at 5 days in the xenograft group ($^{*}P < 0.05$). The mean cumulative decline of signal loss was comparable in all three groups in the first week after transplantation. In the second week post-transplant (day 14) a significant decrease was detected in allograft and xenograft groups ($^{\dagger}P < 0.05$) compared with the isograft group. A significant difference was also found between days 7 and 14, for the allografts and xenograft group ($^{\ddagger}P < 0.05$)

Histology

In Fig. 4, H&E and anti-insulin staining is shown for transplanted PI in livers from each group. Histology showed a well-preserved PI structure, without lymphoid infiltration and with many insulin positive cells (Fig. 4a, d), in livers from mice in the isograft group. In contrast, all stages of PI destruction and lymphoid infiltration were observed within the livers of allografts and xenografts. The morphology of allogeneic and xenogeneic islets, as observed by H&E staining (Fig. 4b, c), was severely impaired; fewer islet cells were detected and a rich lymphocyte infiltration was evident. Immunohistology of allografts and xenografts (Fig. 4e, f) showed fewer insulin positive cells localized within a limited region of the islets and co-localized with regions of cellular infiltration.

Discussion

Our results support the hypothesis that in the first few days after PI transplantation there is a dramatic loss of transplanted tissue [3,5,6]. This is in agreement with a previous MRI study of islet loss during the first 2 weeks post-transplantation [26,27] and with similar studies using other imaging modalities [7,28]. In the Evgenov paper [26] a 2D imaging sequence was employed and 13 MR slices (500 microns each) were used to quantify the number of signal voids in the mouse livers, by manually counting voids. In the Kriz paper [27] a threshold used for detection of transplanted PI was based on the contrast between transplant and nontransplant liver lobes and it was very sensitive to accurate perimeter of these lobes; some of adjacent tissues of liver are hypointensive on MR images (for example lung) and for that cases even small imprecision could significantly affect the number of detected PI. To reduce the imprecision given by subjectivity in manual evaluation we developed an automated method for detection and quantification of transplanted islets in MR images which takes advantage of 3D high resolution image data and which takes into account signal voids present in all images slices to determine the total volume of signal loss. Signal voids were detected only in phantoms containing iron labeled islets and in right liver lobes in mice, which confirms that this method does not produce false positive results. The high signal-to-noise ratio and the high fractional signal loss of the transplanted PI represented by hypointense regions significantly increased the accuracy of segmentation algorithm. The morphological approach used for segmentation is less general than other image enhancement techniques, like linear or nonlinear gray level adjustment. However, it is very suitable when dark objects on brighter image background (or vice-versa) have to be emphasized. The sensitivity of this algorithm used for PI detection rapidly decreases in case of lower fractional signal loss (<30%). Applied morphological operations affect the image only locally (fragments where small bright or dark objects are located), thus it does not modify image gray level distribution as significantly as histogram equalization procedure. The latter, also used for image contrast improvement, is a strongly non-liner operation which often leads to loss of important image information. Our segmentation technique could be beneficial in clinical practice where islets would presumably be distributed throughout the whole liver and therefore there is no tissue free of signal voids which could be used for manual threshold setting. This automatic segmentation can also be used for the analysis of various types of iron-loaded cells in any tissue, not only PI in the liver.

The interpretation of relative changes is easier if we look at the data week by week than total relative PI signal decline (Table 1). Our results show a substantial loss of PI within the first week post-transplant in allografts, xenografts and isografts, all transplant groups showed a comparable signal loss in day 7. This early loss could be due to damage to the PI during isolation, labeling and transplantation, where

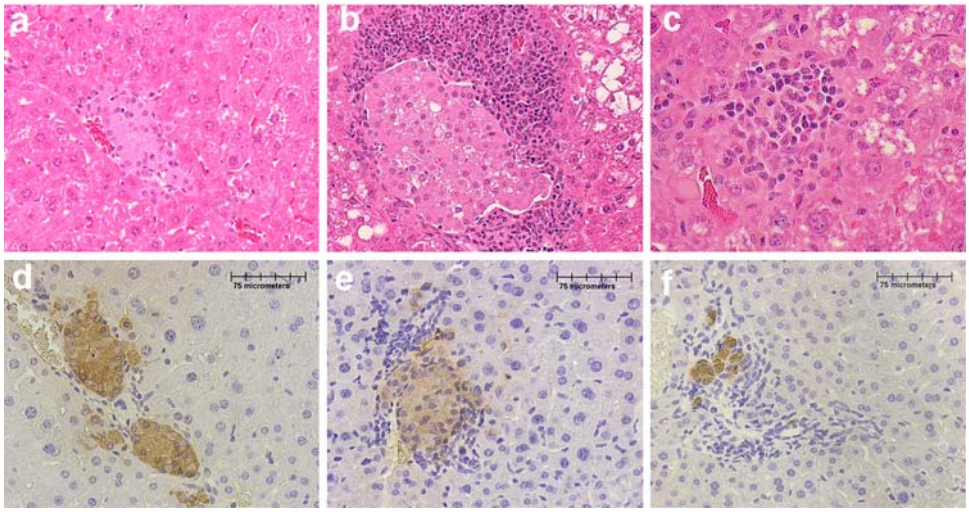

Fig. 4 H&E (**a**–**c**) and anti-insulin (**d**–**f**) staining of the liver containing transplanted islets. Isografts are shown in **a** and **d**, allografts in **b** and **e** and xenografts in **c** and **f**. H&E of the isograft (**a**) shows a well-preserved islet. In contrast H&E of the allograft and xenograft (**b**, **c**) shows massive cellular infiltration and islet destruction. Anti-insulin staining of the isograft shows many insulin positive cells (*brown*), whereas in the allograft (**e**) and xenograft (**f**) fewer insulin positive cells are detected and those that remain are co-localized with regions of immune cell infiltration

PIs are exposed to various insults and toxic stresses (mechanic injury, ischemia, instant blood mediated inflammatory reaction, hyperglycemia) [29]. However, in the second week post-transplant, the transplant animal groups significantly differed.

This suggests that monitoring of PI losses by MRI could begin approximately 1 week post-transplant when the effects of acute rejection dominate. These results are compatible with previously published studies describing the acute rejection of PI after transplantation [30] and its monitoring by MRI [26,31] where it has also been shown that MRI is sensitive to differences in the rates of islet loss for different transplant groups.

Several additional MRI studies have reported that MRI is useful for the detection and monitoring of transplanted islets labeled with SPIO agents and the impact of labeling PI with SPIO has been tested extensively [9–12,26,31–34]. These studies have shown that islet viability, insulin secretion, apoptosis levels and the islet structure as observed by electron and light microscopy are not affected by SPIO labeling at the levels required for detection by MRI. Toso et al. [35] have used SPIO in human diabetic patients. In our study the fact that normoglycemia was restored in diabetic mice after transplantation of SPIO-labeled islets, of relatively low numbers, also demonstrates that labeled islets are functioning normally. There are some limitations of the use of SPIO for islet labeling and tracking by MRI. First, all types of susceptibility artifacts will cause signal loss, including artifacts due to bone, vessels, hemorrhage or local field inhomogeneities. This has the potential to cause false positives, leading to the incorrect identification of voids as PI. The exclusion of above mentioned artifacts is subjective and depends on experience of researcher(s). In this study, manual outlining of the liver was used to minimize the occurrence of these potential false positives.

There are also important points to consider regarding the method of quantifying the islet loss using MRI. The hypointense areas on MR images reflect the presence of iron, not PI. For instance, transplanted PI may be present in the liver as single units or collections of PI of variable sizes and so, the appearance of a discrete void in the image may represent one or more labeled PI. Simply counting the number of voids in a sample of image slices, which was previously the approach of our lab, and others, will suffer from errors related to this clustering. Therefore it is not possible to report absolute values for the number of PI. Furthermore, during the time the iron can be released even from living PI and consequently this islet will not produce hypointense area and therefore will be not detected by any segmentation algorithm. In addition, PI volume measurements made on the first scanning session are different for each animal. This is because of small differences in the numbers of PI arriving into the liver, and because the iron content of each transplanted PI is not identical. To compare differences between imaging timepoints and transplant groups we reported the relative decline in the total volume of signal loss, as a percentage, relative to the first scan. The development of new pulse sequences which generate positive contrast from iron-labeled cells, which is underway, may alleviate this concern [36–38].

Another issue is that the presence of free iron, that might be released from dead or dying PI, may be mistakenly reported as viable islets. Previous work has shown that with PI rejection, after transplantation into the liver, regions of signal loss disappear within days, as they are cleared by resident liver macrophages [26]. A recent paper by Pawelczyk et al. [39], which studied iron uptake by bystander cells in an in vitro model system, indicates that the transfer of iron particles to macrophages, from dead, iron-labeled cells, accounts for $<10\%$ of the total iron in the labeled cells. These data advocate caution since the implantation of iron-labeled cells into tissues can result in uptake of label by macrophages, but suggest that the amount of iron in these cells may be quite low and that SPIO will be quickly degraded by macrophages in the liver. However, in spite of all these problematic points, the advantage of automatic segmentation algorithm is fast quantification of transplanted PI with the same systematic error of hypointense area segmentation which leads to better reproducibility of results. It becomes more important in case of large data set.

Conclusion

Our results on phantoms suggest that the segmentation technique described here allows for the reproducible, more objective assessment of transplanted PI. The quantification of PI is attributed to the combination of high quality image data, a simple and robust automatic segmentation read out and a novel transplant model. The method of transplanting iron-labeled PI into a unambiguously selected portion of the liver allowed for the implementation and optimization of an automatic segmentation technique in case of in vivo experiments for the direct objective quantification of the total area occupied by transplanted PI. We anticipate that this simple and efficient technique will become an accessible tool for the quantification of the fate of cells in a variety of applications for cellular MRI. We have applied our segmentation technique to the detection of transplanted allo-, xeno- and isografts of PI into the liver during the early post-transplant period. Our quantification confirms the hypothesis that a significant number of PI is destroyed in the first week following transplantation irrespective of whether they were allografts, xenografts or isografts. In the second week following transplantation the regions of signal loss due to isografts disappeared more slowly than those representing allografts and xenografts.

Acknowledgments We thank B.K. Rutt and A. Alejski for technical support, V. Herynek for valuable comments and J.A. Snir for assistance with 3D reconstruction. This work was supported by grant from the Canadian Institute of Health Research MOP79547 and by *ENCITE-Seventh Framework Programme, 1M0021620803.*

References

1. Shapiro AM, Lakey JR, Ryan EA, Korbutt GS, Toth E, Warnock GL, Kneteman NM, Rajotte RV (2000) Islet transplantation in seven patients with type 1 diabetes mellitus using a glucocorticoid-free immunosuppressive regimen. N Engl J Med 343:230–238
2. White SA, James RF, Swift SM, Kimber RM, Nicholson ML (2001) Human islet cell transplantation—future prospects. Diabet Med 18:78–103
3. Biarnés M, Montolio M, Nacher V, Raurell M, Soler J, Montanya E (2002) Beta-cell death and mass in syngeneically transplanted islets exposed to short- and long-term hyperglycemia. Diabetes 51:66–72
4. Eich T, Eriksson O, Lundgren T (2007) Nordic network for clinical islet transplantation. Visualization of early engraftment in clinical islet transplantation by positron-emission tomography. N Engl J Med 356:2754–2755
5. Barshes NR, Wyllie S, Goss JA (2005) Inflammation-mediated dysfunction and apoptosis in pancreatic islet transplantation: implications for intrahepatic grafts. J Leukoc Biol 77:587–597
6. Davalli AM, Scaglia L, Zangen DH, Hollister J, Bonner-Weir S, Weir GC (1996) Vulnerability of islets in the immediate post-transplantation period. Dynamic changes in structure and function. Diabetes 45:1161–1167
7. Eich T, Eriksson O, Sundin A, Estrada S, Brandhorst D, Brandhorst H, Langstrom B, Nilsson B, Korsgren O, Lundgren T (2007) Positron emission tomography: a real-time tool to quantify early islet engraftment in a preclinical large animal model. Transplantation 84:893–898
8. Ryan EA, Paty BW, Senior PA, Bigam D, Alfadhli E, Kneteman NM, Lakey JR, Shapiro AM (2005) Five-year follow-up after clinical islet transplantation. Diabetes 54:2060–2069
9. McAteer MA, Sibson NR, von Zur Muhlen C, Schneider JE, Lowe AS, Warrick N, Channon KM, Anthony DC, Choudhury RP (2007) In vivo magnetic resonance imaging of acute brain inflammation using microparticles of iron oxide. Nat Med 13:1253–1258
10. Hsiao JK, Tai MF, Chu HH, Chen ST, Li H, Lai DM, Hsieh ST, Wang JL, Liu HM (2007) Magnetic nanoparticle labeling of mesenchymal stem cells without transfection agent: cellular behavior and capability of detection with clinical 1.5 T magnetic resonance at the single cell level. Magn Reson Med 58:717–724
11. Oweida AJ, Dunn EA, Karlik SJ, Dekaban GA, Foster PJ (2007) Iron-oxide labeling of hematogenous macrophages in a model of experimental autoimmune encephalomyelitis and the contribution to signal loss in fast imaging employing steady state acquisition (FIESTA) images. J Magn Reson Imaging 26:144–151
12. Hauger O, Grenier N, Deminère C, Lasseur C, Delmas Y, Merville P, Combe C (2007) USPIO-enhanced MR imaging of macrophage infiltration in native and transplanted kidneys: initial results in humans. Eur Radiol 17:2898–2907
13. Deux JF, Dai J, Rivière C, Gazeau F, Méric P, Gillet B, Roger J, Pons JN, Letourneur D, Boudghène FP, Allaire E (2008) Aortic aneurysms in a rat model: in vivo MR imaging of endovascular cell therapy. Radiology 246:185–192
14. Heyn C, Ronald JA, Mackenzie LT, MacDonald IC, Chambers AF, Rutt BK, Foster PJ (2006) In vivo magnetic resonance imaging of single cells in mouse brain with optical validation. Magn Reson Med 55:23–29
15. Shapiro EM, Medford-Davis LN, Fahmy TM, Dunbar CE, Koretsky AP (2007) Antibody-mediated cell labeling of peripheral T cells with micron-sized iron oxide particles (MPIOs) allows single cell detection by MRI. Contrast Media Mol Imaging 2:147–153

16. Jirák D, Kríz J, Herynek V, Andersson B, Girman P, Burian M, Saudek F, Hájek M (2004) MRI of transplanted pancreatic islets. Magn Reson Med 52:1228–1233
17. Evgenov NV, Medarova Z, Dai G, Bonner-Weir S, Moore A (2006) In vivo imaging of islet transplantation. Nat Med 12: 144–148
18. Tai JH, Foster P, Rosales A, Feng B, Hasilo C, Martinez V, Ramadan S, Snir J, Melling CW, Dhanvantari S, Rutt B, White DJ (2006) Imaging islets labeled with magnetic nanoparticles at 1.5 Tesla. Diabetes 55:2931–2938
19. Barnett BP, Arepally A, Karmarkar PV, Qian D, Gilson WD, Walczak P, Howland V, Lawler L, Lauzon C, Stuber M, Kraitchman DL, Bulte JW (2007) Magnetic resonance-guided, real-time targeted delivery and imaging of magnetocapsules immunoprotecting pancreatic islet cells. Nat Med 13:986–991
20. Kriz J, Jirak D, White D, Foster P (2008) Magnetic resonance imaging of pancreatic islets transplanted into the right liver lobes of diabetic mice. Transplant Proc 40:444–448
21. Gotoh M, Maki T, Kiyoizumi T, Satomi S, Monaco AP (1985) An improved method for isolation of mouse pancreatic islets. Transplantation 140:437–438
22. Yonekawa Y, Okitsu T, Wake K, Iwanaga Y, Noguchi H, Nagata H, Liu X, Kobayashi N, Matsumoto S (2006) A new mouse model for intraportal islet transplantation with limited hepatic lobe as a graft site. Transplantation 82:712–715
23. Russ JC (2006) The image processing handbook, 5th edn (Image Processing Handbook). CRC, USA
24. Gonzales RC, Woods RE, Eddins SL (2004) Digital image processing using Matlab. Pearson Prentice Hall, New Jersey
25. Inderbitzin D, Gass M, Beldi G, Ayouni E, Nordin A, Sidler D, Gloor B, Candinas D, Stoupis C (2004) Magnetic resonance imaging provides accurate and precise volume determination of the regenerating mouse liver. J Gastrointest Surg 8:806–811
26. Sjögren CE, Johansson C, Naevestad A, Sontum PC, Briley-Saebø K, Fahlvik AK (1997) Crystal size and properties of superparamagnetic iron oxide (SPIO) particles. Magn Reson Imaging 15:55–67
27. Evgenov NV, Medarova Z, Pratt J, Pantazopoulos P, Leyting S, Bonner-Weir S, Moore A (2006) In vivo imaging of immune rejection in transplanted pancreatic islets. Diabetes 55:2419–2428
28. Chen X, Zhang X, Larson CS, Baker MS, Kaufman DB (2006) In vivo bioluminescence imaging of transplanted islets and early detection of graft rejection. Transplantation 81:1421–1427
29. van der Windt DJ, Bottino R, Casu A, Campanile N, Cooper DK (2007) Rapid loss of intraportally transplanted islets: an overview of pathophysiology and preventive strategies. Xenotransplantation 14:288–297
30. Titus T, Badet L, Gray DW (2000) Islet cell transplantation for insulin-dependant diabetes mellitus: perspectives from the present and prospects for the future. Expert Rev Mol Med 2:1–28
31. Kriz J, Jirák D, Girman P, Berková Z, Zacharovova K, Honsova E, Lodererova A, Hajek M, Saudek F (2005) Magnetic resonance imaging of pancreatic islets in tolerance and rejection. Transplantation 80:1596–1603
32. Berkova Z, Kriz J, Girman P, Zacharovova K, Koblas T, Dovolilova E, Saudek F (2005) Vitality of pancreatic islets labeled for magnetic resonance imaging with iron particles. Transplant Proc 37:3496–3498
33. Medarova Z, Evgenov NV, Dai G, Bonner-Weir S, Moore A (2006) In vivo multimodal imaging of transplanted pancreatic islets. Nat Protoc 1:429–435
34. Berkova Z, Jirak D, Zacharovova K, Kriz J, Lodererova A, Girman P, Koblas T, Dovolilova E, Vancova M, Hajek M, Saudek F (2008) Labeling of pancreatic islets with iron oxide nanoparticles for in vivo detection with magnetic resonance. Transplantation 85:155–159
35. Toso C, Vallee JP, Morel P, Ris F, Demuylder-Mischler S, Lepetit-Coiffe M, Marangon N, Saudek F, James Shapiro AM, Bosco D, Berney T (2008) Clinical magnetic resonance imaging of pancreatic islet grafts after iron nanoparticle labeling. Am J Transplant 8:701–706
36. Cunningham CH, Arai T, Yang PC, McConnell MV, Pauly JM, Conolly SM (2005) Positive contrast magnetic resonance imaging of cells labeled with magnetic nanoparticles. Magn Reson Med 53:999–1005
37. Stuber M, Gilson WD, Schär M, Kedziorek DA, Hofmann LV, Shah S, Vonken EJ, Bulte JW, Kraitchman DL (2007) Positive contrast visualization of iron oxide-labeled stem cells using inversion-recovery with ON-resonant water suppression (IRON). Magn Reson Med 58:1072–1077
38. Farrar CT, Dai G, Novikov M, Rosenzweig A, Weissleder R, Rosen BR, Sosnovik DE (2008) Impact of field strength and iron oxide nanoparticle concentration on the linearity and diagnostic accuracy of off-resonance imaging. NMR Biomed 21:453–463
39. Pawelczyk E, Arbab AS, Chaudhry A, Balakumaran A, Robey PG, Frank JA (2008) In vitro model of bromodeoxyuridine or iron oxide nanoparticle uptake by activated macrophages from labeled stem cells: implications for cellular therapy. Stem Cells 5: 1366–1375